J. Fluid Mech. (1978), *vol.* 87, *part* 3, *pp.* 449–474
Printed in Great Britain

Convection in a porous cavity

By KEN L. WALKER AND GEORGE M. HOMSY

Department of Chemical Engineering, Stanford University,
Stanford, California 94305

(Received 27 September 1977)

Convection in a porous cavity driven by heating in the horizontal is analysed by a number of different techniques which yield a fairly complete description of the two-dimensional solutions. The solutions are governed by two dimensionless parameters: the Darcy–Rayleigh number R and the cavity aspect ratio A. We first find solutions valid for shallow cavities, $A \to 0$, by using matched asymptotic expansions. These solutions are given up to $O(A^6R^4)$. For A fixed, we find regular expansions in R by semi-numerical techniques, up to $O(R^{30})$ in some cases. Series-improvement techniques then enable us to cover the range $0 \leqslant R \leqslant \infty$. A limited result regarding bifurcations is noted. Finally, for $R \to \infty$ with A fixed, we propose a self-consistent boundary-layer theory which extends previous approximate work. The results obtained by these different methods of solution are in good agreement with each other and with experiments.

1. Introduction

This work is concerned with the problem of natural convection in a cavity which encloses a Darcy medium. The cavity is heated differentially in the horizontal, and the goal of our analysis is to provide as complete a description as possible of the flow and heat transport across the cavity as a function of the parameters of the problem. We consider here only steady two-dimensional solutions to the governing equations; questions of bifurcation and instability are not treated in any depth.

Convection in porous spaces has been intensively studied over the past few years, most of the effort being focused on the instability problem related to uniform heating from below. See, for example, Horne & O'Sullivan (1974), Caltagirone (1975), Straus (1974) and the review article by Combarnous & Bories (1975). Substantially fewer studies have been made of the present problem. Weber (1975) has presented an approximate boundary-layer analysis and there have been some numerical solutions of questionable accuracy: Bankvall (1974), Holst & Aziz (1972) and Chan, Ivey & Barry (1970). We shall discuss these in §§ 5 and 4 respectively. To our knowledge, there has only been one experimental study which has probed the internal details of the temperature field in a porous cavity. This was done by Klarsfeld (1970), who was able to exploit an interesting technique by which isotherms in a normally opaque medium may be determined by a selective match of the index of refraction between the fluid and the solid medium. There appears, then, to be a gap in our understanding of the convective transport of energy in a porous space heated differentially in the horizontal. The present work seeks to fill that gap in several important respects.

In the next section we state the particular boundary-value problem facing us, and make some comments regarding the validity of some basic assumptions in the writing

of the field equations for porous media. The problem which arises is simple in the sense that it is fully characterized by the aspect ratio of the cavity, denoted by A, and the Darcy–Rayleigh number R. The subsequent sections treat the problem by perturbation theory in the limits of long narrow cavities and low Rayleigh number respectively.

The first case, that of small A with R fixed, results in a problem in matched asymptotic expansions. It is possible to obtain a simple parallel flow solution, valid far from the vertical walls of the cavity, which contains one unknown constant related to the temperature gradient in the core and therefore to the Nusselt number. The evaluation of this constant, and hence the solution to the problem, depends on an analysis of the turning flow which takes place near the vertical boundaries of the cavity. We pursue these calculations to one more order in the small parameter A than we are able to evaluate analytically, $O(A^6)$. Results up to sixth order are then provided by a numerical calculation from a later section.

The next section treats the problem for $A = O(1)$, by regular expansion in R about the state of pure conduction. This approach leads to a series of Poisson problems at each order of the expansion and these are solved sequentially by a semi-numerical method. We focus most of our attention on the resulting series for the Nusselt number. It is found to have only a finite radius of convergence owing to branch cuts in the complex plane which are of no physical significance. Using a variety of techniques common in the physics literature (see, for example, Gaunt & Guttman 1974) and popularized in the fluid-mechanics literature by Van Dyke (1974) and others, it is possible to extend the range of validity of the series over the entire range of Rayleigh numbers $0 \leqslant R \leqslant \infty$. It is, however, difficult to make this extension accurately, and we discuss some of the problems associated with techniques of this kind. The fifth and final section considers the boundary-layer limit for $R \to \infty$ with A fixed. It is shown, by a partial analysis of the horizontal boundary layers, that the approximations due to Gill (1966) and Weber (1975) can be justified and that the conventional vertical boundary-layer equations may be integrated in a straightforward manner. Requiring that these solutions satisfy a consistency relation with the horizontal layers allows us to determine, among other things, the temperature profile along the midplane of the cavity.

2. Basic equations

The problem under study is steady two-dimensional natural convection in a rectangular cavity containing a Darcy medium. The two vertical surfaces are held at fixed but different temperatures and the horizontal surfaces are taken to be perfectly insulating. The momentum boundary conditions are no mass flux through the boundaries. We take the cavity to be of height H and length L, with a co-ordinate system (x, y) centred at the lower left corner. The governing dimensionless equations are

$$\nabla^2 \psi = R\theta_x, \tag{2.1a}$$

$$\nabla^2 \theta = \psi_y \theta_x - \psi_x \theta_y, \tag{2.1b}$$

with the conditions

$$\psi = 0 \quad \text{on} \quad x = 0, 1, \tag{2.2a}$$

$$\psi = 0 \quad \text{on} \quad y = 0, A, \tag{2.2b}$$

$$\theta = x \quad \text{on} \quad x = 0, 1, \tag{2.3a}$$

$$\theta_y = 0 \quad \text{on} \quad y = 0, A. \tag{2.3b}$$

In these equations the subscripts denote partial differentiation. ψ is a stream function defined such that $(u, v) = (\psi_y, -\psi_x)$, and the Boussinesq approximation has been used in writing the momentum equation (2.1 *a*). Lengths have been scaled by L, velocities by K/L and temperatures by the imposed temperature difference ΔT. The resulting problem contains two dimensionless parameters: the aspect ratio $A \equiv H/L$ and the Darcy–Rayleigh number $R \equiv g\alpha\Delta TkL/\nu K$ (k is the permeability of the medium; all other symbols have their usual meaning). We shall have occasion to use also the Rayleigh number $R_H \equiv g\alpha\Delta TkH/\nu K = RA$ based upon the cavity height.

Solutions to this problem are of some interest for very large values of R. However, it is important to note that the porous-media equations (2.1) and (2.2) are invalid for sufficiently large R. Thus the physical applicability of asymptotic solutions to (2.1) and (2.2) valid as $R \to \infty$ is sometimes questionable. There are several reasons for this. Since the permeability k is usully small, a large R often corresponds to a large temperature difference. The variation of fluid properties, especially the viscosity, then becomes quite important; see, for example, Kassoy & Zebib (1975). More important, the Darcy assumption becomes invalid when the heating is so strong that the flow on the microscale is no longer inertialess. This effect can be assessed quantitatively if the solution of (2.1) and (2.2) is coupled with a knowledge of the pore size of a given medium; see, for example, Palm, Weber & Kvernvold (1972). Finally, when the flow is predicted to have a boundary-layer structure, solutions become invalid when rapid variations occur over distances of the same order as the pore size or inter-particle spacing. Thus we shall treat (2.1) as a model system and determine solutions to the stated mathematical problem, which represents a valid approximation to the actual physical system provided that the above considerations are noted.

3. The long shallow cavity

In this section we consider the case $A \to 0$ with R fixed. The treatment is similar in many respects to that given for a viscous Boussinesq fluid by Cormack, Leal & Imberger (1974). As the aspect ratio approaches zero one expects the resistance forces in the centre portion eventually to dominate the flow structure over most of the cavity. Physically this corresponds to a region of dimensional length $O(L)$ of slow nearly parallel flow in the core and a temperature profile only weakly dependent on y, the vertical co-ordinate. The flow then turns through 180° in the end regions. The existence of two different regions with different characteristic horizontal length scales, $O(L)$ in the core and $O(H)$ at the ends, suggests a matched asymptotic expansion in the aspect ratio A.

It is convenient, then, to work with a set of dimensionless variables scaled in a way which reflects these general expectations. In the core, i.e. the region removed from vertical boundaries, we scale y with H, x with L and ψ with A^2RK/L. It is furthermore advantageous to base the Rayleigh number on the height: $R_H = AR$. With these scalings, the core field equations become

$$\nabla_A^2 \psi_c = \theta_{cx}, \tag{3.1 a}$$

$$\nabla_A^2 \theta_c = A^2 R_H(\psi_{cy}\theta_{cx} - \psi_{cx}\theta_{cy}), \tag{3.1 b}$$

$$\nabla_A^2 \equiv \partial^2/\partial y^2 + A^2\,\partial^2/\partial x^2, \tag{3.1 c}$$

with

$$\psi_c = \theta_{cy} = 0 \quad \text{on} \quad y = 0, 1 \tag{3.1 d}$$

and conditions, to be determined below, matching the core solution to solutions valid at the ends of the cavity. These equations admit a parallel flow solution $\psi = \psi_c(y)$ of the form

$$\psi_c(y) = \tfrac{1}{2}C(y^2 - y), \tag{3.2}$$

$$\theta_c(x, y) = \{Cx + D + \tfrac{1}{2}R_H A^2 C^2(\tfrac{1}{3}y^3 - \tfrac{1}{2}y^2)\}. \tag{3.3}$$

Here C and D are unknown constants of integration. (These solutions may be developed, as in Cormack *et al.* (1974), by expansion in A. They are simply recorded here.) The parallel flow solution is, of course, not uniformly valid, and must be corrected in the corner regions by fields which allow the flow to turn. The details of the turning flow, together with matching conditions, will determine the constants C and D. Before proceeding, it is advantageous to eliminate the constant D in favour of C. This may be done if the core temperature is specified at any point (x, y). We appeal to the invariance of the governing equations to double reflexions about diagonals passing through the centre of the cavity (the so-called 'centro-symmetry' of the problem; Gill 1966) to conclude that $\theta_c(\frac{1}{2}, \frac{1}{2}) = \frac{1}{2}$. From this relation we find

$$D = \tfrac{1}{2} - \tfrac{1}{2}C + \tfrac{1}{24}R_H A^2 C^2$$

and therefore $$\theta_c(x, y) = \{\tfrac{1}{2}(1 - C) + Cx + \tfrac{1}{2}R_H A^2 C^2(\tfrac{1}{3}y^3 - \tfrac{1}{2}y^2 + \tfrac{1}{12})\}. \tag{3.4}$$

Thus the core solution is given by (3.2) and (3.4) in terms of a single unknown constant C, to be determined by matching. We assume the following asymptotic expansion for C:

$$C(R, A) = C_0(R) + AC_1(R) + A^2 C_2(R) + \ldots \quad \text{as} \quad A \to 0 \quad \text{with} \quad R \quad \text{fixed}. \tag{3.5}$$

This choice of gauge functions is justified if it is possible to obtain proper matching with the end regions.

The end region at $x = 0$ is now considered in order to evaluate the coefficients C_i. It is necessary to consider only one of the two end regions owing to the centro-symmetry of the problem. Thus we consider solutions $(\hat{\theta}, \hat{\psi})$ valid in the region $0 \leqslant x \sim A$, $0 \leqslant y \leqslant 1$. For $0 \leqslant x \sim A$, the equations satisfied by $(\hat{\theta}, \hat{\psi})$ are

$$A\nabla^2\hat{\psi} = \hat{\theta}_x, \tag{3.6a}$$

$$\nabla^2\hat{\theta} = AR_H(\hat{\psi}_y\hat{\theta}_x - \hat{\psi}_x\hat{\theta}_y), \tag{3.6b}$$

subject to the boundary conditions

$$\hat{\theta}(0, y) = 0, \quad \hat{\psi}(0, y) = 0, \tag{3.7a, b}$$

$$\hat{\theta}_y = \hat{\psi} = 0 \quad \text{on} \quad y = 0, 1 \tag{3.7c}$$

and the matching conditions

$$\lim_{x\to\infty} \hat{\theta}(x, y) = \lim_{x\to 0} \theta_c(x, y), \quad \lim_{x\to\infty} \hat{\psi}(x, y) = \lim_{x\to 0} \psi_c(x, y). \tag{3.7d}$$

The limits in (3.7*d*) are to be interpreted in the sense of matched asymptotic expansions, applied to the m-term asymptotic expansion of each of the end and core variables in the small parameter A.

Solutions to the corner problems are likewise expressed as asymptotic expansions in A; viz.

$$\hat{\theta} = \hat{\theta}_0 + A\hat{\theta}_1 + \ldots, \quad \hat{\psi} = \hat{\psi}_0 + A\hat{\psi}_1 + \ldots. \tag{3.8}$$

Substitution into (3.1) and (3.2) gives the following problems for $\hat{\theta}_0$, $\hat{\psi}_0$, etc., subject to the homogeneous conditions (3.7a, b, c) at each order:

$$\left.\begin{aligned} \partial\hat{\theta}_0/\partial x = 0, \quad \nabla^2\hat{\theta}_0 = 0, \\ \lim_{x\to\infty}\hat{\theta}_0 = \tfrac{1}{2}(1-C_0); \end{aligned}\right\} \tag{3.9}$$

$$\left.\begin{aligned} \nabla^2\hat{\psi}_0 = \partial\hat{\theta}_1/\partial x, \quad \nabla^2\hat{\theta}_1 = R_H\,\partial(\hat{\psi}_0,\hat{\theta}_0)/\partial(x,y), \\ \lim_{x\to\infty}\hat{\psi}_0 = \tfrac{1}{2}C_0(y^2-y), \quad \lim_{x\to\infty}\hat{\theta}_1 = (C_0\,x - \tfrac{1}{2}C_1); \end{aligned}\right\} \tag{3.10}$$

$$\left.\begin{aligned} \nabla^2\hat{\psi}_1 = \partial\hat{\theta}_2/\partial x, \quad \nabla^2\hat{\theta}_2 = R_H[\partial(\hat{\theta}_0,\hat{\psi}_1)/\partial(x,y) + \partial(\hat{\theta}_1,\hat{\psi}_0)/\partial(x,y)], \\ \lim_{x\to\infty}\hat{\psi}_1 = \tfrac{1}{2}C_1(y^2-y), \quad \lim_{x\to\infty}\hat{\theta}_2 = C_1 x - \tfrac{1}{2}C_2 + \tfrac{1}{2}R_H C_0^2(\tfrac{1}{3}y^3 - \tfrac{1}{2}y^3 + \tfrac{1}{12}). \end{aligned}\right\} \tag{3.11}$$

The first two temperature functions may be obtained by inspection. Thus, since matching at each order gives the constants $C_0, C_1, \ldots$, $\hat{\theta}_0 = 0$ yields $C_0 = 1$ and $\hat{\theta}_1 = x$ yields $C_1 = 0$.

The constant C_2 may be evaluated by a symmetry argument. First, from (3.10), $\hat{\psi}_0$ will be a symmetric function of y. However $\hat{\psi}_2$ will contain both symmetric and antisymmetric parts owing to the matching in (3.11). Letting $\hat{\theta}_2 = \hat{\theta}_{2A} + \hat{\theta}_{2S}$ gives

$$\left.\begin{aligned} \nabla^2\hat{\theta}_{2A} = \hat{\psi}_{0y}, \\ \lim_{x\to\infty}\hat{\theta}_{2A} = \tfrac{1}{2}R_H(\tfrac{1}{3}y^3 - \tfrac{1}{2}y^2 + \tfrac{1}{12}), \end{aligned}\right\} \tag{3.12}$$

$$\left.\begin{aligned} \nabla^2\hat{\theta}_{2S} = 0, \quad \lim_{x\to\infty}\hat{\theta}_{2S} = -\tfrac{1}{2}C_2, \\ \hat{\theta}_{2S} = 0 \quad \text{on} \quad x = 0, \quad \partial\hat{\theta}_{2S}/\partial y = 0 \quad \text{on} \quad y = 0, 1. \end{aligned}\right\} \tag{3.13}$$

Equations (3.13) have the solution $\hat{\theta}_{2S} \equiv 0$, with the consequence that $C_2 \equiv 0$. A similar argument may be used to show that $C_4 \equiv 0$.

The solutions for $\hat{\psi}_0$ and $\hat{\theta}_2$ are

$$\hat{\psi}_0 = \tfrac{1}{2}(y^2-y) + \sum_{n\,\text{odd}} (4/n^3\pi^3)\sin(n\pi y)\,e^{-n\pi x}, \tag{3.14}$$

$$\hat{\theta}_2 = \hat{\theta}_{2A} = \tfrac{1}{2}R_H(\tfrac{1}{3}y^3 - \tfrac{1}{2}y^2 + \tfrac{1}{12}) - R_H \sum_{n\,\text{odd}} \left(\frac{2x}{n^3\pi^3} + \frac{4}{n^4\pi^4}\right)\cos(n\pi y)\,e^{-n\pi x}. \tag{3.15}$$

Knowledge of the solution thus far allows determination of the constant C_3. The problem for $\hat{\theta}_3$ is

$$\left.\begin{aligned} \nabla^2\hat{\theta}_3 = R_H[\partial\psi_1/\partial y + \partial(\hat{\theta}_2,\hat{\psi}_0)/\partial(x,y)], \\ \lim_{x\to\infty}\hat{\theta}_3 = -\tfrac{1}{2}C_3, \\ \partial\hat{\theta}_3/\partial y = 0 \quad \text{on} \quad y = 0, 1, \\ \hat{\theta}_3 = 0 \quad \text{on} \quad x = 0. \end{aligned}\right\} \tag{3.16}$$

The constant C_3 is clearly related to the part of $\hat{\theta}_3$ which is even in y. Letting

$$z(x) \equiv \int_0^1 \hat{\theta}_3\,dy,$$

one can show that

$$C_3 = -2\lim_{x\to\infty} z(x) = -R_H^2\frac{30}{\pi^7}\sum_{n\,\text{odd}} n^{-7} \cong -9{\cdot}9374921\times 10^{-3}R_H^2.$$

All the higher-order C_k are also related to the symmetric parts of the $\hat{\theta}_k$, and it is possible to show by the same methods that

$$C_5 = O(R_H^4), \quad C_6 = 3C_3^2, \quad C_7 = O(R_H^6), \quad C_8 = 8C_3C_5$$

and so on. Knowledge of an odd C_k immediately gives the next even C_k.

It is difficult to proceed analytically beyond the present results, i.e. beyond C_4. We wish to use these results to calculate an asymptotic expansion for the Nusselt number† valid for $A \to 0$ with R fixed. One method of doing this is a direct evaluation of the flux from the wall at $x = 0$, as in Cormack *et al.* (1974), viz.

$$Nu^* = \int_0^1 \frac{\partial \hat{\theta}}{\partial x}\bigg|_{x=0} dy = \sum A^k \int_0^1 \frac{\partial \hat{\theta}_k}{\partial x}\bigg|_{x=0} dy.$$

We choose instead a rather simple method which relies on the fact that the horizontal walls are insulated, and hence the flux across any vertical cross-section is constant. In particular, this flux may be calculated directly from the core solution as

$$Nu = \int_0^1 \left(\frac{\partial \theta_c}{\partial x} - R_H \frac{\partial \psi_c}{\partial y}\theta_c\right) dy. \tag{3.17}$$

Using (3.4) and (3.6), we find

$$Nu = AC[1 + \tfrac{1}{120} R_H^2 A^2 C^2]. \tag{3.18}$$

Equation (3.18) is exact for any aspect ratio for which the parallel flow solution is valid: this implies $A < 1$, since tall cavities cannot be expected to have this simple core solution. Knowledge of the constant C, or its expansion in A, completes the solution. Evaluating this expression up to $O(A^6)$, with

$$C = 1 + A^3 R_H^2 \hat{C}_3 + R_H^4 A^5(\hat{C}_5 + 3\hat{C}_3^2 A) + O(A^7 R_H^6),$$

we find

$$Nu = A[1 + A^2 R_H^2(\tfrac{1}{120} + \hat{C}_3 A) + A^5 R_H^4(\hat{C}_5 + \tfrac{1}{40}\hat{C}_3 + 3\hat{C}_3^2 A) + O(A^7)]. \tag{3.19}$$

Note that we have used the relation $C_6 = 3C_3^2$, and have written $C_3 = \hat{C}_3 R_H^2$, $\hat{C}_3 = -9{\cdot}9374921 \times 10^{-3}$ and $C_5 = \hat{C}_5 R_H^4$. We are at present unable to evaluate $\hat{C}_5$ analytically. We shall return to this in § 4.6, where we evaluate $\hat{C}_5$ numerically.

4. Convection for $A = O(1)$: solution by regular expansion in R

4.1. *The expansion*

We return to the problem stated in § 2, viz. (2.1)–(2.3). It is possible to solve these equations as a regular expansion in R, i.e.

$$\theta = \sum_{s=0}^{S} \theta^s(x, y) R^s, \quad \psi = \sum_{s=0}^{S} \psi^s(x, y) R^s. \tag{4.1}$$

† Note that here and throughout this paper the Nusselt number is based on the height H, i.e. $Nu = qH/k\Delta T$.

It is trivial to show that $\theta^0 = x$ and $\psi^0 = 0$. Thus the expansion is about the state of simple conduction. The expansions (4.1) lead to a sequence of Poisson problems for the successive $\theta^s(x, y)$ and $\psi^s(x, y)$:

$$\nabla^2 \psi^s = \theta_x^{s-1}, \tag{4.2a}$$

$$\nabla^2 \theta^s = \sum_{r=1}^{s} (\psi_y^r \theta_x^{s-r} - \psi_x^r \theta_y^{s-r}) \quad \text{for} \quad s \geqslant 1, \tag{4.2b}$$

$$\left.\begin{aligned} \theta^s = \psi^s = 0 \quad &\text{on} \quad x = 0, 1 \\ \theta_y^s = \psi^s = 0 \quad &\text{on} \quad y = 0, A \end{aligned}\right\} \quad \text{for} \quad s \geqslant 1. \tag{4.2c}$$

These Poisson problems may be solved in a variety of ways:† we have chosen a Galerkin method using truncated spectral representations, viz.

$$\theta^s(x, y) = \sum_{n=0}^{N} \sum_{m=1}^{M} \theta_{m,n}^s \sin(m\pi x) \cos(n\pi y/A), \tag{4.3a}$$

$$\psi^s(x, y) = \sum_{n=1}^{N} \sum_{m=1}^{M} \psi_{m,n}^s \sin(m\pi x) \sin(n\pi y/A). \tag{4.3b}$$

The matrices of the coefficients $\theta_{m,n}^s$ and $\psi_{m,n}^s$ are found by requiring (4.3) to solve (4.2*a*, *b*) in the sense of weighted residuals. There is a great deal of symmetry in this problem, which is reflected in the matrices: it is easy to show that each function θ^s is odd (even) in x and even (odd) in y when s is an odd (even) integer. This implies that non-zero values of $\theta_{m,n}^s$ occur only when m and n are either both odd or both even. Similar considerations apply to $\psi_{m,n}^s$, and this symmetry was exploited in determining the matrices numerically.

A double-precision Fortran program was written which evaluated these coefficient matrices for a given choice of M, N and S. It consists essentially of six nested DO loops for calculating the quantities $\theta_{m,n}^s$ and $\psi_{m,n}^s$.

Two quantities of primary interest are the Nusselt number, which because of the symmetry becomes

$$Nu = A \sum_{n=0}^{\frac{1}{2}S} c_n R^{2n} \tag{4.4}$$

(where $c_0 = 1$), and the value of the stream function at the cavity centre,

$$\psi(\tfrac{1}{2}, \tfrac{1}{2}A) = \sum_{n=0}^{\frac{1}{2}S} e_n R^{2n+1}, \tag{4.5}$$

which is related to the strength of the circulation in the core. From the spectral representations, we have

$$c_n = \sum_{m=2}^{M} (m\pi) \theta_{m,0}^{2n}, \tag{4.6}$$

$$e_n = \sum_{k=1}^{M} \sum_{l=1}^{N} \psi_{k,l}^{2n+1} \sin\left(\frac{k\pi}{2}\right) \sin\left(\frac{l\pi}{2}\right). \tag{4.7}$$

As we shall see, the accuracy of these results is of crucial importance for the utility of a series like (4.4) or (4.5). A discussion of accuracy is given in the appendix. The coefficients c_n and e_n are given for different values of A in tables 1 and 2 respectively.

† See appendix for discussion.

$\frac{1}{2}S$	$A = 1$ (20, 20)	$A = 2$ (30, 20)	$A = 3$ (36, 26)
0	1·0	1·0	1·0
1	8·51247 (−04)	9·18364 (−04)	6·58217 (−04)
2	−6·85672 (−07)	−8·30023 (−07)	−5·19226 (−07)
3	9·41183 (−10)	1·22260 (−09)	7·21572 (−10)
4	−1·54846 (−12)	−2·16607 (−12)	−1·23480 (−12)
5	2·79626 (−15)	4·22836 (−15)	2·34042 (−15)
6	−5·35023 (−18)	−8·76313 (−18)	−4·71414 (−18)
7	1·06521 (−20)	1·89164 (−20)	9·89169 (−21)
8	−2·18346 (−23)	−4·20609 (−23)	−2·13805 (−23)
9	4·57665 (−26)	9·56555 (−26)	4·72689 (−26)
10	−9·76379 (−29)	−2·21440 (−28)	−1·06383 (−28)
11	2·11308 (−31)	5·20053 (−31)	2·42908 (−31)
12	−4·62773 (−34)	−1·23594 (−33)	−5·61298 (−34)
13	1·02368 (−36)	2·96677 (−36)	1·31011 (−36)
14	−2·28385 (−39)	−7·18239 (−39)	—
15	5·13302 (−42)	1·75165 (−41)	—
16	−1·16111 (−44)	−4·29939 (−44)	—
17	2·64142 (−47)	1·06125 (−46)	—
18	−6·03925 (−50)	−2·63268 (−49)	—
19	1·38701 (−52)	6·56022 (−52)	—
20	−3·19836 (−55)	−1·64127 (−54)	—
	$\epsilon_0 = 402{\cdot}02500$	$\epsilon_0 = 370{\cdot}700$	$\epsilon_0 = 381{\cdot}092$

TABLE 1. Coefficients of $Nu = A \sum_{n=0}^{\frac{1}{2}S} c_n R^{2n}$.

$\frac{1}{2}S$	$A = 1$ (20, 20)	$A = 2$ (30, 20)	$A = 3$ (36, 26)
0	7·36556 (−02)	1·13842 (−01)	1·22714 (−01)
1	−2·08049 (−05)	−2·14162 (−05)	−8·64608 (−06)
2	2·41158 (−08)	2·30308 (−08)	4·56956 (−09)
3	−3·64799 (−11)	−3·64713 (−11)	−5·73122 (−12)
4	6·24787 (−14)	6·75114 (−14)	1·01854 (−14)
5	−1·15235 (−16)	−1·35763 (−16)	−2·03926 (−17)
6	2·23331 (−19)	2·87464 (−19)	4·29734 (−20)
7	−4·48464 (−22)	−6·30645 (−22)	−9·33450 (−23)
8	9·24891 (−25)	1·42003 (−24)	2·07232 (−25)
9	−1·94749 (−27)	−3·26216 (−27)	−4·68008 (−28)
10	4·16952 (−30)	7·61431 (−30)	1·07177 (−30)
11	−9·04923 (−33)	−1·80052 (−32)	−2·48300 (−33)
12	1·98641 (−35)	4·30389 (−35)	5·80902 (−36)
13	−4·40250 (−38)	−1·03824 (−37)	—
14	9·83802 (−41)	2·52431 (−40)	—
15	−2·21421 (−43)	−6·17936 (−43)	—
16	5·01468 (−46)	1·52172 (−45)	—
17	−1·14199 (−48)	−3·76713 (−48)	—
18	2·61343 (−51)	9·36967 (−51)	—
19	−6·00711 (−54)	−2·34025 (−53)	—
	$\epsilon_0 = 402{\cdot}025$	$\epsilon_0 = 370{\cdot}697$	$\epsilon_0 = 381{\cdot}255$

TABLE 2. Coefficients of $\psi_c = \sum_{n=0}^{\frac{1}{2}S} e_n R^{2n+1}$.

4.2. *Range of validity of the series*

Series such as (4.4) have, in general, a limited radius of convergence, and therefore a limited utility for description of the physical quantity of interest. There seems to be no generalization possible at the moment, but the limited radius of convergence is often due to the presence of a pole or branch point located, in general, in the complex plane of the expansion variable (the Rayleigh number in this case). The pole may be of physical significance, indicating a point of bifurcation or in some cases the non-existence of solutions; it may, however, lie on the imaginary axis, and therefore have no physical significance. For examples of all these possibilities, see Van Dyke (1974, 1977). The singularity closest to the origin in the complex plane determines the radius of convergence, and its nature and location may be determined by the use of a simple graphical test due to Domb & Sykes (1957). Functions $f(x)$ of the form

$$f(x) = \text{constant}\,(1+x/\epsilon_0)^{\alpha} \tag{4.8a}$$

will, from the binomial expansion, have Taylor coefficients which behave like

$$a_n = \frac{c_n}{c_{n-1}} = -\frac{1}{\epsilon_0}\left(1-\frac{1+\alpha}{n}\right). \tag{4.8b}$$

The coefficients of series like (4.4) will ultimately be dominated by the nearest singularity, so we expect (4.8) to hold for sufficiently large n. (Here it is implicitly assumed that the structure of the solution is indeed that of (4.8a). See Stewartson (1976) for a counter-example and discussion.) The exponent α and the location ϵ_0 of the singularity are determined from the asymptotic behaviour of the Domb–Sykes coefficients a_n:

$$\lim_{1/n\to 0} a_n = \frac{1}{\epsilon_0}, \quad \lim_{1/n\to 0} \frac{da_n}{d(1/n)} = \frac{1+\alpha}{\epsilon_0}.$$

This determination is often done graphically using a Domb–Sykes plot of a_n versus $1/n$. The intercept yields the location of the singularity closest to the origin and the value of the exponent can be calculated from the slope as $1/n \to 0$. The coefficients α and ϵ_0 can also be determined with greater accuracy by using higher-order interpolation methods to extrapolate to $1/n = 0$. Figure 1 shows the Domb–Sykes plot for $A = 2$. For this and the other aspect ratios studied, a square-root singularity ($\alpha = 0{\cdot}50$) is found at a negative value of R^2, e.g. $\epsilon_0 = R^2 = -370{\cdot}70$ for $A = 2$. (Recall that the series for the Nusselt number involves only even powers of the Rayleigh number; hence $x = R^2$ here.) A singularity lying on the negative real axis, thus corresponding to an imaginary Rayleigh number, has no physical significance and unnecessarily limits the range of applicability of the series. There are several possible ways in which the radius of convergence can be extended, depending on the nature of the singularity. If the first singularity is multiplicative a new series for $Nu(\epsilon_0+R^2)^{-\frac{1}{2}}$ can be formed which has a larger radius of convergence. By factorizing out this first singularity it was found that the new series has a singularity at the same location with an exponent of $-0{\cdot}50$, indicating that the first singularity is not multiplicative. Another possibility is that the singularity is additive; however, on subtracting out the first singularity, the new series $Nu - a_1(\epsilon_0+R^2)^{0{\cdot}50}$ has a singularity at the same location with an exponent of $1{\cdot}50$. By continuing this process of subtracting out singularities as long as accuracy

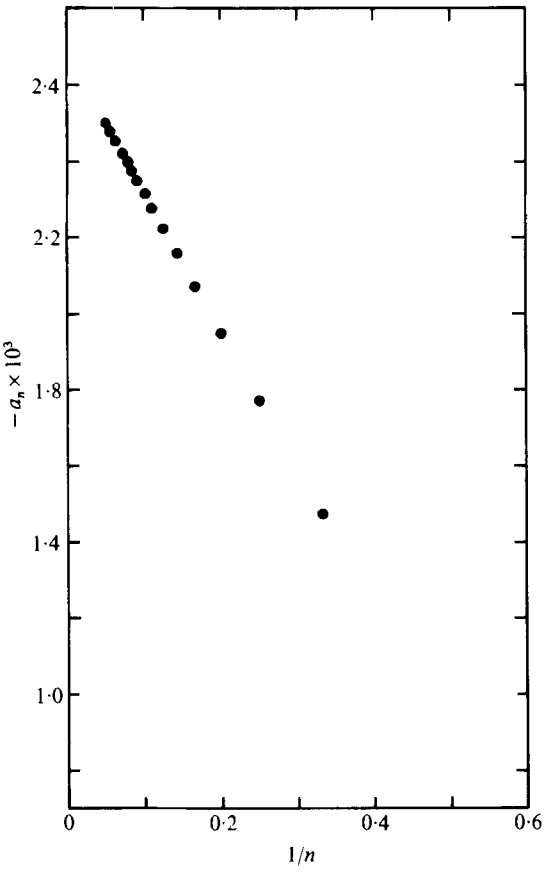

FIGURE 1. The Domb–Sykes plot for the series (4.4).

allowed, it was found that each subtraction resulted in a new series with a singularity at the same location and an exponent equal to the previous value plus one. This indicates that the series for the Nusselt number is of the form

$$Nu(R^2) = (R^2+\epsilon_0)^{0\cdot5} A(y) + B(R^2), \tag{4.9}$$

where $y = R^2+\epsilon_0$ and A and B are entire functions of their arguments. We have been unable to determine the forms of the functions A and B, so it is difficult to extract much useful information from the series in their original forms.

The series for the value of the stream function in the core exhibits a singularity of the same nature and at the same location as does the series for Nu. However, since the stream function, is a point quantity, the coefficients are known with less accuracy than those for Nu and no relation similar to (4.9) could be ascertained.

The locations of the singularities are noted in table 1 and in each case occur for such low values of R^2 ($R \sim 20i$) that the practical utility of the original series is severely limited. We next discuss extensions.

4.3. *Extension of range of validity*

The immediate goal is to extend the radius of convergence of the series. For a complete discussion of most of the methods used, the reader is referred to Gaunt & Guttmann

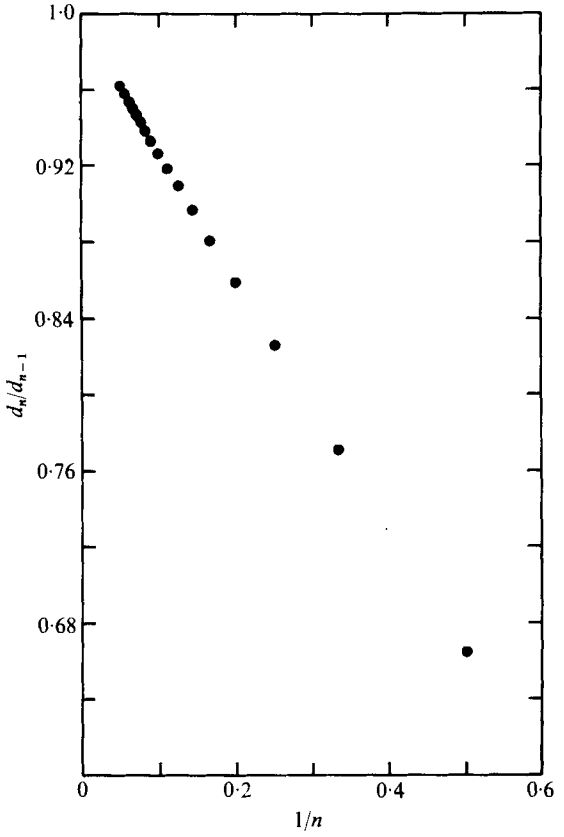

FIGURE 2. The Domb–Sykes plot for the Euler series (4.11).

(1974) and Van Dyke (1974, 1977). The Nusselt number series for a rectangular cavity with an aspect ratio of two will be discussed first. Unless noted otherwise the discussion will refer to the numerical results for $M = 30$ and $N = 20$.

Assuming, as in the present case, that the non-analytic term may be neither subtracted nor divided out, it is common to use the Euler transformation to map the nearest singularity to infinity. Thus by definition of the new ('Euler') variable

$$z \equiv R^2/(R^2+c_0), \tag{4.10}$$

a new series may be determined; e.g.

$$Nu = \Sigma d_n z^n, \tag{4.11}$$

where the d_n are determined from the c_n by comparing the two series (4.11) and (4.4). The properties of the series (4.11) are now of interest. We have used variations of three techniques to study (4.11).

First, figure 2 shows the Domb–Sykes plot for this series. It is seen that the extrapolation to $1/n = 0$ indicates an intercept of nearly 1·0. (In the Euler variable, $R^2 = \infty$ corresponds to $z = 1$; if this is the location of the next singularity, it indicates extension of the original series to $R = \infty$.) It is at this point that the limited accuracy of the d_n, due to the truncated spectral representations, makes itself felt. In fact, we shall see

(M, N)	Linear	Quadratic	Cubic
(20, 12)	0·99694	0·99868	0·99914
(24, 16)	0·99740	0·99923	0·99968
(30, 20)	0·99776	0·99971	1·0002

TABLE 3. Intercepts of Domb–Sykes plots of Euler series for $Nu(z)$ (up to order R^{28}).

the numerical accuracy degenerate as we attempt to determine respectively the location, nature and amplitude of the next singularity.

Table 3 gives the results of analysis of the intercepts from the Domb–Sykes plot for series valid up to R^{28}, with the intercepts evaluated by linear, quadratic and cubic fits to the last points. It is seen that, as the spectral resolution increases, the estimates of the intercept approach 1·0, and it is therefore possible to conclude that, to the available numerical accuracy, the Euler transformation extends the radius of convergence of (4.4) to all Rayleigh numbers.

At this point we may state a restricted result regarding bifurcations. Since the Nusselt number (and indeed other point quantities such as the stream function at the cavity centre) is a single-valued function of R^2, one may conclude that there are no *steady two-dimensional* flows which bifurcate from the unicellular flow computed here. This is not to say, however, that this flow is stable for all R, since the restricted result makes no statement regarding bifurcations to time-dependent or three-dimensional motions.

Even though the radius of convergence has been extended to a very large if not infinite Rayleigh number, the utility of the Euler series (4.11) for direct evaluation of the heat transport is severely limited. The reason for this is the slow convergence of (4.11) for Rayleigh numbers of physical interest, i.e. for z approaching 1. The analytical nature of the singularity at infinity is therefore of some interest. If we assume that the series (4.11) does converge for $0 \leqslant z \leqslant 1$ and that the asymptotic form is algebraic, i.e.

$$Nu \sim (1-z)^{\alpha} \quad \text{as} \quad z \to 1, \tag{4.12a}$$

then we see that in terms of the physical variables

$$Nu \sim \epsilon_0^{\alpha} R^{-2\alpha} \quad \text{as} \quad R \to \infty. \tag{4.12b}$$

The exponent α and the leading constant in (4.12b) are therefore of great interest. We first discuss the exponent α. Of course the straightforward way of determining α is by evaluating the slope of the Domb–Sykes plot, figure 2. This proved to be difficult to do accurately, however, because of numerical inaccuracies due to the truncated spectral representations. The Domb–Sykes plots exhibit a mild curvature at low $1/n$ which seems to be related to the number of terms in the expansion in both R *and* Fourier modes. For example, the estimates for α at orders R^{30}, R^{36}, R^{40} are

$$-0{\cdot}257, \; -0{\cdot}251, \; -0{\cdot}249,$$

respectively, for linear extrapolations,

$$-0{\cdot}227, \; -0{\cdot}226, \; -0{\cdot}226$$

for quadratic extrapolations and

$$-0{\cdot}224, \; -0{\cdot}225, \; -0{\cdot}226$$

for cubic extrapolations for the case $M = 30, N = 20$. At $O(R^{30})$, for a coarser spectral representation, $M = 24$, $N = 16$, we find estimates of

$$-0{\cdot}254, \quad -0{\cdot}220, \quad -0{\cdot}211$$

for linear, quadratic and cubic extrapolations. Thus it is difficult to determine α in as satisfactory a manner as we should like.

Another method commonly used to determine the exponent of algebraic forms involves the use of the logarithmic derivative of the Euler series (4.11); see, for example, Gaunt & Guttman (1974) and Van Dyke (1978). From (4.12*a*) it is easy to see that

$$\frac{d}{dz}\ln(1-z)^{\alpha} \sim \frac{\alpha}{1-z} \quad \text{as} \quad z \to 1 \tag{4.13}$$

and the singularity at infinity becomes a simple pole. The series formed by taking $d[\ln(4.11)]/dz$ exhibited a straight Domb–Sykes plot with intercept $1{\cdot}0 \pm 0{\cdot}00001$ and a slope $-0{\cdot}992$ (compared with the expected value of -1). The constant α may then be estimated by computing the ratio of the coefficients of the logarithmic derivative of (4.11) to those of the binomial expansion of $(1-z)^{-1}$. This results in estimates (at R^{30}) of

$$-0{\cdot}231, \quad -0{\cdot}234, \quad -0{\cdot}232$$

from linear, quadratic and cubic extrapolations, respectively. Attempts to use Padé approximants to mimic (4.13) led to erratic estimates for α which did not provide support for any particular value.

All the evidence, taken together, supports a value for α between $-0{\cdot}25$ and $-0{\cdot}23$. Without the benefit of any further information, we should be led to accept a value slightly less than $-\frac{1}{4}$. However, asymptotic analysis in terms of boundary-layer theory (§ 5) supports the value of $-\frac{1}{4}$, indicating that the Nusselt number goes as $R^{\frac{1}{2}}$ for large R; cf. (4.12*b*). Giving the corroborating boundary-layer theory, we thus conclude that $\alpha = -\frac{1}{4}$ and that the numerical inaccuracies are due to the limited spectral representation in the higher terms in the expansion in R.

Having determined that the Euler series for the Nusselt number has a singularity at $z = 1$ ($R = \infty$) and is asymptotic to $(1-z)^{-\frac{1}{4}}$, it remains to estimate the leading numerical coefficient, often called the 'amplitude'; see Gaunt & Guttman (1974). In what follows we refer to the amplitude as the coefficient written in the physical variables, i.e. we write

$$Nu = hR^{\frac{1}{2}} \quad \text{as} \quad R \to \infty \tag{4.14}$$

and estimate h.

The amplitude of the square-root singularity at infinity can be determined using either the Euler series or Padé approximants of the original series. In the first method, one forms the ratio of the Euler coefficients d_n in (4.11) to those of the binomial expansion of $(1-z)^{-\frac{1}{4}}$. These estimates, expressed as h, are given in table 4, together with results for other values of A, and clearly converge to a value near 0·357 for $A = 2$. These data extrapolate to $0{\cdot}36 \pm 0{\cdot}005$.

The amplitude can also be estimated using the $[N+1/N]$ Padé approximant to the fourth power of the original series (4.4), i.e.

$$Nu^4_{[N+1/N]} \equiv p_{N+1}(x)/q_N(x) \quad \text{where} \quad x = R^2, \tag{4.15}$$

$\frac{1}{2}S$	$A = 1$ (20, 20)	$A = 2$ (30, 20)	$A = 3$ (20, 20)
1	0·3057	0·3103	0·2272
5	0·3682	0·3488	0·2892
10	0·4007	0·3560	0·3058
15	0·4190	0·3574	0·3080
20	0·4302	0·3574	—
25	0·4373	—	—

TABLE 4. Estimates of amplitude h.

where $p(x)$ and $q(x)$ are polynomial functions of their arguments with coefficients chosen such that (4.15) agrees with the series (4.4) raised to the fourth power to order $\frac{1}{2}S$ in x. By working with Nu^4, the correct asymptotic behaviour is guaranteed. The amplitude is then estimated as the ratio of the coefficient of the highest power of x in $p_{N+1}(x)$ to that in $q_N(x)$. The idea behind this approach has been suggested by Baker (1965) and recently amplified by Frost & Harper (1976), who give many examples. We had only limited success with the method for this problem. The estimates for h based on [6/5], [7/6], etc. approximants were 0·312, 0·315, 0·317, 0·318 and 0·319, indicating that they converge slowly, if at all. A sensitivity analysis was performed and it was found that the behaviour of the $[N+1/N]$ approximants was extremely sensitive to small errors in the higher coefficients of the series for Nu^4.

It is possible, of course, to construct Padé approximants for Nu provided that both the amplitude and the strength of the singularity at infinity are known. This involves solution of a set of (often ill-conditioned) linear equations; see Frost & Harper (1976). The results have great utility in engineering work, providing a closed-form rational fraction for $Nu(R)$ which may be easily evaluated.

In addition, the Nusselt number may be calculated directly from the truncated Euler series provided that z is not close to 1. For large R, resulting in $z \to 1$, we may also attempt to complete the series by construction of a 'mimic' function; see Van Dyke (1974) and Gaunt & Guttman (1974). A truncated series with S terms can be completed by assuming that the remaining terms are proportional to the coefficients of the series representation of a function chosen to correspond to a prescribed asymptotic behaviour. A slight disadvantage is that the mimic function takes on an amplitude determined entirely by the value of the last coefficient in the Euler series; see Van Dyke (1974, § 5.2). When the series is reasonably well behaved this is not a problem, but in some cases (see table 4) one loses the benefit of extrapolation. On the basis of the above discussion, the mimic function for $A = 2$ is

$$Nu = 0{\cdot}357(1-z)^{-\frac{1}{4}} + \sum_{s=0}^{20} d_s z^s. \tag{4.16}$$

We shall compare the mimic function, the Padé approximants and the available numerical calculations in § 4.5 below.

4.4. *Stream function*

Another quantity of interest is the value of the stream function at the cavity centre and its dependence on R. The centre value of the stream function is related to the

circulation which is driven by the buoyancy. As mentioned earlier, the fact that the coefficients in the series for the stream function are known to less accuracy than those in the Nusselt number series makes an analysis of the asymptotic behaviour more difficult. We shall again discuss the case $A = 2$, $(M, N) = (30, 20)$ for definiteness. It is convenient to treat the series for ψ_c/R obtained from (4.5), i.e.

$$\psi/R = \sum_{n=0}^{\frac{1}{2}S} e_n x^n \quad \text{where} \quad x = R^2. \tag{4.17}$$

This series has a branch cut of the same nature and at the same location as does the series for the Nusselt number. As before, an Euler transformation is used to extend the radius of convergence. The resulting Euler series has a singularity at $z = 1{\cdot}001$ and again with increased accuracy this singularity moves closer to $z = 1$, leading to the conclusion that the Euler series has a radius of convergence of infinity in the physical variable. Subsequent determination of the exponent of the singularity and its amplitude by any of the techniques described above proved difficult to accomplish to any satisfactory degree. For example the last few estimates of the slope from the Domb–Sykes plots were (up to R^{38})

$$0{\cdot}48,\ 0{\cdot}41,\ 0{\cdot}35,\ 0{\cdot}29,$$

whereas the logarithmic derivative gave, for the same quantity,

$$0{\cdot}192,\ 0{\cdot}192,\ 0{\cdot}193,\ 0{\cdot}194$$

and the $[N/N+1]$ Padé approximants yielded (recall that the singularity is a simple pole, which accounts for the choice of order of the approximants)

$$0{\cdot}195,\ 0{\cdot}202,\ 0{\cdot}207,\ 0{\cdot}212.$$

All these data suggest, but certainly do not conclusively indicate, a value of $\frac{1}{4}$, which would imply that

$$\psi(\tfrac{1}{2}, \tfrac{1}{2}A) \sim kR^{\frac{1}{2}} \quad \text{as} \quad R \to \infty. \tag{4.18}$$

We do not have the numerical accuracy necessary to prove (4.18). It will emerge below, however, that this asymptotic behaviour for $\psi(\frac{1}{2}, \frac{1}{2}A)$ is consistent with a boundary-layer model due to Gill (1966) and Weber (1975) and refined by us.

The amplitude k corresponding to the asymptotic form was estimated as

$$1{\cdot}048,\ 1{\cdot}071,\ 1{\cdot}096,\ 1{\cdot}11$$

by forming the ratios of Euler coefficients to corresponding coefficients in the expansion of $(1-z)^{\frac{1}{4}}$. The amplitude was also estimated by $[N/N+1]$ Padé approximants for the series for $(\psi/R)^4$ and yielded

$$0{\cdot}896,\ 0{\cdot}912,\ 0{\cdot}925,\ 0{\cdot}935,$$

which are slightly lower than, but consistent with, the values given above.

4.5. *Summary of results*

The discussion up to this point has almost entirely concerned the Nusselt number for a cavity of aspect ratio 2. We now briefly discuss other quantities and other aspect ratios, and compare the predictions with available numerical results.

For other aspect ratios, the asymptotic behaviour proved difficult to determine. Refer, for example, to table 4. The need for greater accuracy and more terms is

		k	
A	h	Padé	Domb–Sykes
1	0·47	0·66	0·41
2	0·360	1·00	0·8
3	0·31	1·26	0·9

TABLE 5. Amplitudes h and k for asymptotic behaviour of Nu and ψ_c respectively.

R	Mimic function	Padé	Finite difference
	$A = 1$		
25	1·38	1·38	1·11†
—	—	—	1·37‡
50	1·98	1·98	1·99†
—	—	—	2·15‡
—	—	—	2·34§
—	—	—	2·1*
100	3·091	3·097	3·56‡
			3·5*
200	4·84	4·89	4·89†
500	8·4	8·66	8·78†
1000	12·49	12·96	—
	$A = 2$		
25	2·79	2·79	2·84†
—	—	—	2·86‡
50	3·95	3·95	4·3‡
100	5·90	5·90	6·1†
—	—	—	6·7‡
500	14·67	14·67	15·6†
1000	21·3	21·4	—

† Horne (1975). § Holst & Aziz (1972).
‡ Chan *et al.* (1970). * Bankvall (1974).

TABLE 6. Comparison of Nusselt numbers computed by different methods.

probably due to increased importance of other singularities at $z = 1$. A boundary-layer analysis (§ 5) predicts that

$$Nu = hR^{\frac{1}{2}} + \sum_{M=1}^{\infty} a_M f_M(R).$$

A probable choice for the gauge functions is (see below)

$$Nu = hR^{\frac{1}{2}} + R^{\frac{1}{2}} \sum_{M=1}^{\infty} a_M R^{-\frac{1}{4}M}$$

and in terms of the Euler variable this corresponds to

$$Nu = \alpha_0(1-z)^{-\frac{1}{4}} + \sum_{M=1}^{\infty} \alpha_M (1-z)^{-\frac{1}{4}+\frac{1}{8}M}.$$

The magnitude of α_M compared with α_0, especially for small M, will determine how many terms in the Rayleigh number expansion are needed in order to observe the $R^{\frac{1}{2}}$ dependence. Table 5 succinctly summarizes the results regarding the asymptotic

$O(R^2)$	$A = \frac{1}{4}$	$A = \frac{1}{8}$
Regular expansion	2·28485 (−6)	5·15194 (−6)
Equation (3.19) with $\hat{C}_3 = -9{\cdot}937494 \times 10^{-3}$	2·28475 (−6)	5·15207 (−6)
$O(R^4)$		
Regular expansion	−2·83982 (−10)	−9·8178 (−12)
$\hat{C}_5$ using (3.19)	0·9993 (−4)	1·0012 (−4)

TABLE 7. Coefficients of Nu/A at $O(R^2)$ and $O(R^4)$ for small A. $(M, N) = (16, 98)$.

behaviour of both the stream function at the cavity centre and the Nusselt number. The preceding discussion has amply indicated the poor accuracy of the former quantity: we have had to rely on extrapolation techniques and for this reason we give results for the amplitude k obtained both from Padé approximants of the original series and Domb–Sykes coefficients from the Euler series. The discrepancy is a measure of the uncertainty in this quantity. Table 6 gives a summary of our results for the Nusselt number at various values of R and a comparison with available numerical results of Horne (1975), Holst & Aziz (1972), Chan *et al.* (1970) and Bankvall (1974). In making this comparison, we point out that with the exception of that by Horne, who used up to 33×65 points, these numerical computations were done on extremely coarse grids (typically 10×10 points) and become suspect for moderate R. It is a general feature of these numerical results that Nu decreases with increasing resolution. For $R \leqslant 100$, our results are in substantial agreement with previous work. For $R > 500$ there are *no* reliable numerical results. Our results obtained using the mimic function and the Padé approximants (chosen to have the correct asymptotic behaviour as $R \to \infty$) are in agreement for moderate R, but diverge slightly at large R. This is because mimic functions such as (4.16) are unduly sensitive to the value of the last Euler coefficient and do not benefit from the extrapolation implied in the values of h recorded in table 5.

4.6. *A numerical evaluation of* $\hat{C}_5$

We now wish to return briefly to the discussion in § 3, where we developed asymptotic results for shallow cavities in the limit $A \to 0$ with R fixed. The main result is (3.19), which expresses the Nusselt number as an asymptotic expansion in A. It is seen that the series formally breaks down when $R^4A^6 = O(1)$. We can, of course, treat the problem through regular expansions in R with A small, but fixed, to verify (3.19) and evaluate the coefficient $\hat{C}_5$ numerically. This was done by using very high spectral representations in (4.3), but taking the expansion in R only to $O(R^4)$. Table 7 verifies that the $O(R^2)$ coefficient is accurately reproduced by the regular expansion series, and examination of the coefficient of R^4 as a function of A and comparison with the expected form from (3.19) show that $\hat{C}_5 \approx 1{\cdot}000 \times 10^{-4}$. This completes the solution for shallow cavities up to $O(A^6)$.

5. A consistent boundary-layer theory

This section discusses the cavity problem in the limit of infinite Rayleigh number and finite aspect ratio in the context of boundary-layer theory. For this case we are performing an expansion about $1/R = 0$, in contrast to $R = 0$ for the regular expansion and $A = 0$ for the singular expansion in the two previous sections. As the Rayleigh number tends towards infinity the heat transfer between the two vertical walls is dominated by convection. Heat transfer by conduction is assumed to be important only in thin boundary layers adjacent to the horizontal and vertical walls.

There has been a small amount of previous work on the boundary-layer limit, notably by Gill (1966) for a cavity containing a viscous fluid. His theory, in all its essential details, has been carried over to the porous cavity by Weber (1975). The theory as developed there suffers from two shortcomings. The first is that no attempt is made to link the solution valid in boundary layers near the vertical walls to the details of the flow across the horizontal surfaces. Plausible arguments leading to the conclusion that the flux of fluid is carried entirely by the cross-flow in core regions have been given by Gill (1966), used by Weber (1975) and recently discussed by Quon (1977). The ambiguity regarding the inability to construct a self-consistent boundary-layer theory which includes the horizontal layers has led previous workers to conclude, incorrectly, that the theory is valid only in the double limit $A \to \infty$, $R \to \infty$, in which case consideration of the horizontal surfaces becomes a moot point. Below we develop such a self-consistent theory for a porous cavity valid in the limit of $R \to \infty$ with A fixed. Similar considerations should be possible for a viscous fluid.

The second shortcoming of the Gill–Weber theory is the crude manner in which the boundary-layer equations were integrated. Thus it is difficult to explain unambiguously discrepancies between theory and either experiment or numerical work; see especially Quon (1977). Below we integrate the boundary-layer equations numerically: this is a straightforward and routine calculation.

It is convenient, though not necessary, to change the scalings of the dimensionless variables somewhat. We scale all lengths with respect to the height and rescale the temperature such that it varies from 1 at the left boundary to 0 at the right. Thus we have

$$\nabla^2\psi = -R_H\theta_x, \quad \nabla^2\theta = \psi_y\theta_x - \psi_x\theta_y, \tag{5.1a,b}$$

$$\left.\begin{aligned} &\psi = 0, \quad \partial\theta/\partial y = 0 \quad \text{on} \quad y = 0, 1, \\ &\theta = 1, \quad \psi = 0 \quad \text{on} \quad x = 0, \\ &\theta = 0, \quad \psi = 0 \quad \text{on} \quad x = 1/A. \end{aligned}\right\} \tag{5.2}$$

We proceed to construct boundary-layer solutions to the problem by first determining the scalings appropriate to the side-wall layers. Next we discuss allowable forms of the 'core' variables, valid in regions removed from boundaries, and the coupling between them and the vertical boundary-layer equations. We next demonstrate the ability to construct a self-consistent closure which includes horizontal layers, and close with some numerical results and comparisons with previous work.

The magnitudes of the characteristic horizontal length and stream function in the vertical boundary layer can be determined in the usual way by balancing convection and conduction in (5.1*b*), balancing buoyancy and vorticity in (5.1*a*), and assuming

that the variation in the x direction is much more rapid than that in the vertical direction. It is found that $\partial/\partial x = O(R_H^{\frac{1}{2}}), \quad \psi = O(R_H^{\frac{1}{2}}),$

yielding the usual boundary-layer equations

$$\Psi_{XX} = -\theta_X, \quad \theta_{XX} = \Psi_y \theta_X - \Psi_X \theta_y \tag{5.3a,b}$$

$$\theta = 1, \quad \Psi = 0 \quad \text{on} \quad X = 0, \tag{5.4}$$

together with matching conditions valid as $X \to \infty$ and a consistent initial condition on θ and Ψ at $y = 0$. Because of the centro-symmetry, it suffices to treat the vertical layer near $x = 0$. Here Ψ and X are boundary-layer variables related to ψ and x through the scalings $R_H^{\frac{1}{2}}$ and $R_H^{-\frac{1}{2}}$ respectively. These equations are valid near the vertical surfaces except at distances of order $R_H^{-\alpha}$ ($\alpha > 0$) from the corners, where the assumption that the characteristic horizontal length is much smaller than the characteristic vertical length does not hold. From the scalings used it can be seen that the vertical boundary layer will provide an $O(R_H^{\frac{1}{2}})$ contribution to the Nusselt number. Since the vertical characteristic length in the corners is vanishingly small compared with that for the boundary layer, it is expected that the corners will give a higher-order correction to the Nusselt number. Thus if one determines the temperature distribution in the boundary layer, it is then possible to calculate the Nusselt number to $O(R_H^{\frac{1}{2}})$. The side-wall solution is of course coupled to the core solution, valid as $X \to \infty$, and dependent upon the prescribed initial data at $y = 0$. We first consider the core variables.

The core region is studied by expressing the core functions as asymptotic expansions:

$$\left.\begin{aligned} \theta^c &= \theta_0^c + R_H^{-\frac{1}{2}} \theta_1^c + R_H^{-\frac{1}{2}} \theta_2^c + \ldots, \\ \Psi^c &= R_H^{\frac{1}{2}} \Psi_0^c + R_H^{\frac{1}{2}} \Psi_1^c + \Psi_2^c + \ldots . \end{aligned}\right\} \tag{5.5}$$

The choice of the gauge functions is not obvious at this point, but is dictated by the form of the horizontal layers. We confine our attention to the leading terms in (5.5), denoted simply by the superscript c.

It is assumed that the characteristic horizontal and vertical lengths are both order one (specifically $\partial/\partial x \sim 1/A$, $\partial/\partial y \sim 1$). Substituting the expansions into the governing equations and equating terms of order $R_H^{\frac{1}{2}}$, it is found that

$$\theta_x^c = 0, \quad \Psi_x^c \theta_y^c = 0, \tag{5.6a,b}$$

which implies

$$\theta^c = \theta^c(y), \quad \Psi^c = \Psi^c(y). \tag{5.7}$$

Owing to the centro-symmetry of the equations, θ^c must be odd in y and Ψ^c must be even about the cavity centre $y = \frac{1}{2}$, or

$$\theta^c(y) = 1 - \theta^c(1-y), \quad \Psi^c(y) = \Psi^c(1-y).$$

This is the only information yielded by the core equations; thus the matching conditions appropriate to (5.3) are

$$\theta \to \theta^c(y), \quad \Psi_X \to 0 \quad \text{as} \quad X \to \infty, \tag{5.8}$$

where $\theta^c(y)$ must be specified. (Note this problem has the feature common to boundary layers that the entrainment velocity, related to $\Psi^c(y)$, cannot be specified, but is obtained as a result of calculation.)

The class of admissible core temperature profiles and the initial data at $y = 0$ are intimately connected with the details of the horizontal layers. It is not our intention to give an exhaustive treatment of this problem, but we have considered what is perhaps the simplest model for the structure. In this model, the convective flux of fluid driven by the buoyancy is carried *entirely* by the cross-flow in the core. Thus $\Psi^c(0) = \Psi^c(1) = 0$ is a constraint on the solution.† Without going into extensive detail (but see the discussion following (5.10) below), it is possible to show that the only core temperature profile compatible with this hypothesis is one in which the temperature of the fluid along the horizontal walls of the cavity is the same as that of the vertical surface from which it has just exited. In the present context, this implies that

$$\theta^c(0) = 0, \quad \theta^c(1) = 1. \tag{5.9}$$

Thus we are led to consider for $\theta^c(y)$ the class of odd functions satisfying (5.9). This function will, in general, have a non-zero derivative at the top and bottom of the cavity; thus $[\partial\theta^c/\partial y]_{y=0,1}$ is an $O(1)$ quantity. For consistency, this necessitates a thin horizontal layer in which convection balances conduction in order that the temperature gradient may vary from zero on the surface to an order-one value to match with the core solution. With the scalings

$$\tilde{y} = R_H^{\alpha} y, \quad \theta^H = R_H^{\gamma}\theta, \quad \Psi^H = R_H^{-\beta}\Psi, \quad \tilde{x} = x \tag{5.10}$$

for the bottom layer, a balance between conduction and convection yields

$$R_H^{2\alpha-\gamma}\theta^H_{\tilde{y}\tilde{y}} = R_H^{\beta+\alpha-\gamma}[\theta^H_{\tilde{x}}\Psi^H_{\tilde{y}} - \theta^H_{\tilde{y}}\Psi^H_{\tilde{x}}],$$

which implies that $\alpha = \beta$. (Conduction is of course the physical mechanism which permits the transition in the slope of the temperature.) Now the matching condition

$$\lim_{\tilde{y}\to\infty} (R_H^{\alpha-\gamma}\,\partial\theta^H/\partial\tilde{y}) = O(1) \tag{5.11}$$

requires $\gamma = \alpha$, and hence $\alpha = \beta = \gamma$. The vorticity equation in this layer is

$$R^{2\alpha+\beta}\Psi^H_{\tilde{y}\tilde{y}} = R^{1-\gamma}\theta^H_{\tilde{x}}.$$

A balance between vorticity and its production then results in $\alpha = \beta = \gamma = \frac{1}{4}$. Thus the mass flux and the temperature in this horizontal layer are both smaller, by a factor of $R^{-\frac{1}{4}}$, than they are in the core. The fact that the equations in this horizontal layer are of fourth order in $\tilde{y}$ indicates the ability to solve them subject to the boundary conditions at $\tilde{y} = 0$ and matching conditions with the core as $\tilde{y}\to\infty$. The fact that this can be accomplished, at least in principle, lends support to the main hypothesis and (5.9). We need not discuss the horizontal layers in further detail, since they do not affect our analysis to leading order, but we do wish to comment that further progress would appear to require not only higher-order boundary-layer theory in the core and vertical layers, but also consideration of the small $O(R_H^{-\frac{1}{4}}) \times O(R_H^{-\frac{1}{4}})$ corner regions of overlap between vertical and horizontal layers.

To summarize, we postulate a model in which the flux of fluid is conveyed entirely by entrainment and detrainment in the vertical layers. (The boundary layer 'empties',

† We refer to this assumption as the main hypothesis. It is the same as that used by Gill, but we go one step further in showing that it is fully consistent with a structure for the horizontal layers and with 'exact' numerical calculations.

to use Gill's phrase.) This in turn leads to the conclusion that the core temperature profile must obey (5.9). The $O(1)$ discontinuity in the temperature gradient at the top and bottom is relaxed by relatively thick, $O(R_H^{-\frac{1}{4}})$ layers in which the temperature and stream function are both of higher order in an expansion in $R_H^{-\frac{1}{4}}$ than the leading terms in the core and side-wall layers. *Self-consistency* of the model then follows *if it is possible* to find functions $\theta^c(y)$ which are odd in y, satisfy $\theta^c(0) = 0$ and $\theta^c(1) = 1$, but are otherwise arbitrary, and which result, through integration of the vertical boundary-layer equations, in predictions for $\Psi^c(y)$ which are symmetric about $y = \frac{1}{2}$ and vanish at $y = 0, 1$.

Returning to the vertical layers, it is possible to eliminate the temperature by first integrating the momentum equation once to give

$$\Psi_X = -\theta + \theta^c(y) \tag{5.12}$$

and substituting into the energy equation to obtain for Ψ

$$\Psi_{XXX} = \Psi_{XX}\Psi_y + \Psi_X(\theta_y^c - \Psi_{Xy}), \tag{5.13}$$

$$\left.\begin{aligned} \Psi_X = \theta^c(y) - 1, \quad \Psi = 0 \quad \text{on} \quad X = 0, \\ \Psi_X = 0 \quad \text{as} \quad X \to \infty. \end{aligned}\right\} \tag{5.14}$$

The method of solving the boundary-layer equations numerically will be discussed briefly before addressing the problem of determining the core temperature and initial conditions at $y = 0$. The boundary-layer equations are recast into Blasius co-ordinates using a Levy–Lees transformation. The transformed variables and equations are

$$\left.\begin{aligned} (X, y) \to (\eta, y) \quad \text{where} \quad \eta = X/y^{\frac{1}{2}}, \\ \Psi_{\eta\eta\eta} = y\theta_y^c(y)\Psi_\eta + y^{\frac{1}{2}}(\Psi_{\eta\eta}\Psi_y - \Psi_\eta\Psi_{\eta y}) + \tfrac{1}{2}y^{-\frac{1}{2}}(\Psi_\eta)^2, \end{aligned}\right\} \tag{5.15}$$

$$\left.\begin{aligned} \Psi = 0, \quad \Psi_\eta = y^{\frac{1}{2}}(\theta^c - 1) \quad \text{on} \quad \eta = 0, \\ \Psi_\eta \to 0 \quad \text{as} \quad \eta \to \infty. \end{aligned}\right\} \tag{5.16}$$

As is well known, a constant temperature at infinity (θ^c = constant) yields a similarity solution with $\Psi(X, y) = y^{\frac{1}{2}}\Psi(\eta)$. There is no guarantee, however, that this is the correct initial condition for the integration of the vertical layers. As fluid with the temperature of the wall from which it came sweeps across the horizontal wall, there is a compression of isotherms into the small square regions of dimensions $O(R_H^{-\frac{1}{4}})$ mentioned above. The solution in this corner region then furnishes the true initial condition for the vertical layer. Because of the structure of the boundary-layer model and the use of η, y variables, it is probable that the solution near $y = 0$ will be approximately the similarity solution. We compared the solutions obtained using these and other initial data and found that the predicted $\Psi^c(y)$ was relatively insensitive to the choice. In general different initial conditions resulted in absolute differences of less than 5 %, except near $y = 0$. This is not surprising since it is characteristic of parabolic equations that the influence of initial conditions tends to die out far from $y = 0$. In all the numerical work reported here we used the similarity solution to provide the necessary initial data.

Equation (5.15) was solved numerically using a finite-difference technique, with central differences for derivatives with respect to η and backward differences for derivatives with respect to y. The method is second-order accurate in both η and y. The

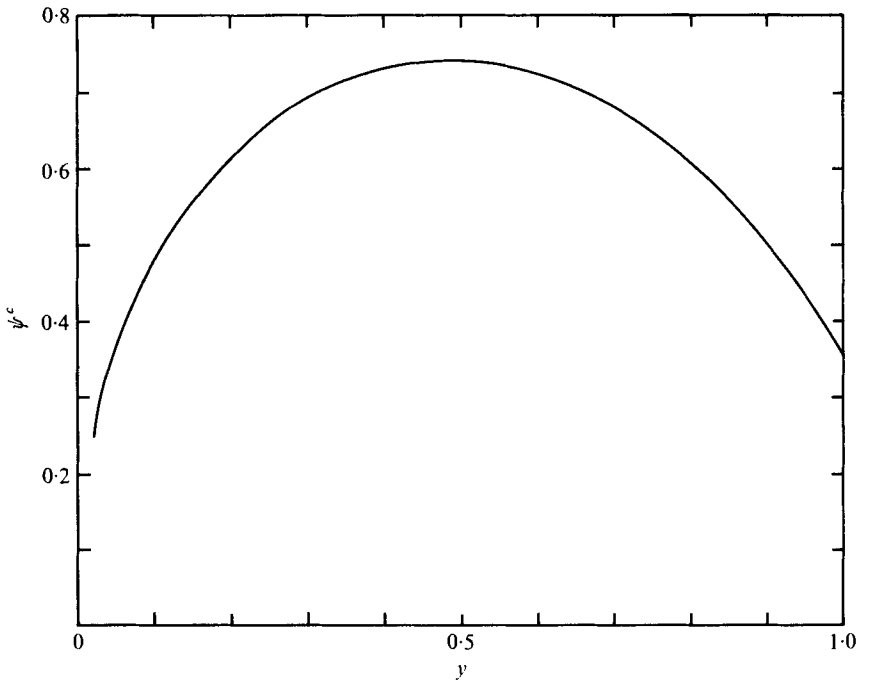

FIGURE 3. $\Psi^c(y)$ for a linear core temperature. $\theta^c(y) = 0{\cdot}77y + 0{\cdot}115$.

equation was solved by stepping in y, i.e. the solution at y used the solution at $y - \Delta y$ and $y - 2\Delta y$. At a given value of y the solution was found by the following iteration scheme:

$$U^M_{\eta\eta} = y\theta^c_y(y)\, U^M + y^{\frac{1}{2}}(U^M_\eta \Psi^{M-1}_y - U^{M-1}U^M_y) + \tfrac{1}{2}y^{-\frac{1}{2}}\, U^M U^{M-1}, \tag{5.17}$$

where $U \equiv \Psi'_\eta$. Discretization results in a tridiagonal system of equations for U^M, and Ψ'^M was then found by quadrature. The iteration process was continued until the relative difference between two iterations was less than a specified tolerance. The boundary condition at infinity was applied at a large but finite value of η

$$(\eta = \eta_T = 10 \sim 15).$$

The parameters Δy, $\Delta\eta$ and η_T were varied to ascertain that the solution was independent of these numerical parameters. Because backward differences were used in the vertical direction, the initial profile had to be specified at two rows in order to start the calculations.

We now discuss the choice of the function $\theta^c(y)$. We first performed some numerical experiments to investigate the close coupling between the main hypothesis that $\Psi^c(0) = \Psi^c(1) = 0$ and the conclusion that θ^c satisfies (5.9). Figure 3 shows the predictions for $\Psi^c(y)$ for a profile $\theta^c(y) = 0{\cdot}77y + 0{\cdot}115$. (This is the only *linear* temperature profile that results in a symmetric Ψ^c.) It is seen that in this case $\Psi^c(1) \neq 0$, which, if accepted, implies that some of the flux is carried by a horizontal layer. But the hypothesis $\Psi' = O(R_H^{\frac{1}{2}})$ in that layer, together with the scalings discussed after (5.10), leads to the contradictory result that the temperature suffers an $O(1)$ jump, which in turn implies an $O(R_H^{\alpha})$ heat flux, which, for $\alpha > 0$, cannot be relaxed to zero by any self-consistent scaling. In addition, the boundary-layer equations themselves suggest

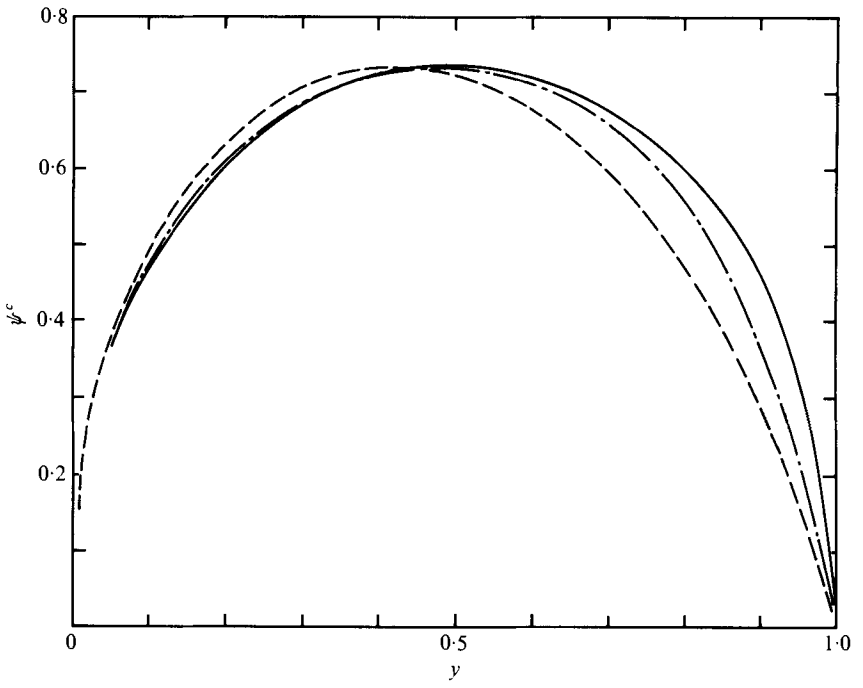

FIGURE 4. $\Psi^c(y)$ for various G and N. ——, $N = 4$, $G = 0{\cdot}77$; – –, $N = 2$, $G = 0{\cdot}77$; – – –, $N = 1$, $G = 1$.

that the main hypothesis implies (5.9), since as $\theta_c \to 1{\cdot}0$ (5.16) become homogeneous, which suggests that, as the circulation loses the buoyancy which drives it, it should relax to zero.

The core temperature profile, in addition to being antisymmetric about $y = \frac{1}{2}$ and varying between zero and one, must also be chosen such that the resulting core stream function is symmetric. The symmetry of the stream function was found to be strongly dependent on the shape of the assumed core temperature profile. We examined the family of odd polynomials of the form

$$\theta^c - \tfrac{1}{2}[1 + G(2y-1) + (1-G)(2y-1)^{2N+1}] \tag{5.18}$$

for various N and G.† Here G is the value of the gradient at the centre. As N increases, the deviation from a linear profile becomes more and more localized near the two horizontal surfaces. Figure 4 shows a few of the calculated results for Ψ^c for various N and G. For a symmetric profile the maximum will occur at $y = \frac{1}{2}$, i.e. the boundary layer entrains fluid in the lower half of the cavity and ejects fluid in the upper half. The location of the maximum was found to depend primarily on the temperature gradient in the centre of the cavity and only weakly on the shape of the core temperature profile or on the initial conditions. A value of G approximately equal to 0·75 results in the maximum being located at $y = \frac{1}{2}$. This choice also results in stream-function profiles that are nearly symmetric except near the horizontal surfaces. For fixed G, we varied

† A few solutions using complete sets of odd polynomials yielded essentially the same results as (5.18).

N in order to find the value resulting in a nearly symmetric $\Psi_c(y)$. The best choice was found to be $N = 4$.

Having found a self-consistent boundary-layer solution, it is possible to evaluate both the value of the stream function at the cavity centre (directly from figure 4) and the Nusselt number (obtained by numerical quadrature). We find, therefore, the asymptotic results

$$\left.\begin{aligned} Nu &= (0{\cdot}51 \pm 0{\cdot}01)\, R^{\frac{1}{2}} A^{-\frac{1}{2}} \\ \Psi^c &= -(0{\cdot}733 \pm 0{\cdot}003)\, A^{\frac{1}{2}} R^{\frac{1}{2}} \\ [\partial\theta^c/\partial y]_{y=0} &= 0{\cdot}75 \end{aligned}\right\} \quad \text{as} \quad R \to \infty, \text{ with } A \text{ fixed.} \tag{5.19}$$

(Note that we have reverted to R, which is based upon L, for comparison with certain of the results from earlier sections.)

The results for the Nusselt number and the centre value of the stream function are in good agreement with the results from the regular expansion for $A = 2$ and 3 (see table 6). The discrepancy for an aspect ratio of one is thought to be due to the difficulties in extracting the asymptotic limit from the regular expansion. The results can also be compared with those of Weber (1975). For the quantities in (5.19), he found

$$Nu = 0{\cdot}58 R^{\frac{1}{2}} A^{-\frac{1}{2}}, \quad \Psi^c = 0{\cdot}87 A^{\frac{1}{2}} R^{\frac{1}{2}}, \quad [\partial\theta^c/\partial y]_{y=0} = \tfrac{2}{3},$$

which, while inaccurate, are surprisingly close to our values considering the approximations which he made.

The most detailed experimental study is that by Klarsfeld (1970). Using the so-called 'Christiansen effect' (see, for example, Cloupeau & Klarsfeld 1973), by which the isotherms may be determined using colour photography, he presented results for a heated cavity over the range $40 \leqslant R \leqslant 1622$ for two aspect ratios: $A = 2{\cdot}25$ and $4{\cdot}5$. His results clearly show the boundary-layer regime for $R_H > 700$ and dramatically demonstrate the existence of the thick, $O(R_H^{-\frac{1}{4}})$ horizontal layers. For the highest Rayleigh numbers which he studied, the isotherms away from the horizontal walls are nearly flat and the core temperature profile is in excellent agreement with that determined here. In figure 5 we have plotted his experimental points together with (5.18) with $G = 0{\cdot}75$ and $N = 4$. The agreement is exact to within the accuracy of the experiments.

We wish to thank Professor Milton Van Dyke for helpful discussions on the content of § 4, Professor Andreas Acrivos for his characteristically clever resolution, via (3.17), of what initially seemed to us to be a paradox and Professor R. Horne for discussions of his numerical calculations. Financial support through NSF-ENG-73-03955 is gratefully acknowledged.

Appendix. Accuracy of regular expansion

It was not our intention to make a detailed comparison of various methods of solving the sequence of Poisson problems arising in § 4. There exist, for example, more efficient ways of evaluating the nonlinear source terms using fast Fourier transforms and a discrete set of points in physical space. Accuracy, not speed, was our main

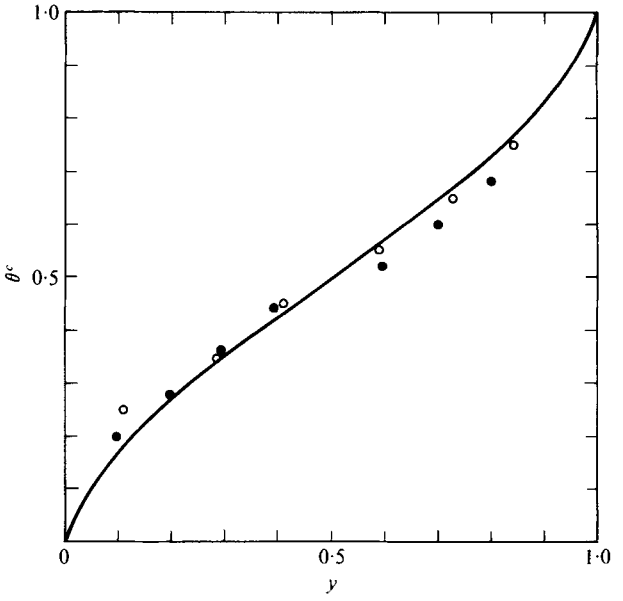

FIGURE 5. $\theta^c(y)$ compared with experiments. ●, $A = 2{\cdot}25$, $R = 1622$; ○, $A = 2{\cdot}25$, $R = 1298$.

Direct Poisson solver		Galerkin	
Mesh size	e_1	Spectral resolution	e_1
8×16	1·13426 (−01)	—	—
16×32	1·13760 (−01)	(24, 16)	1·13806 (−01)
32×64	1·13844 (−01)	(30, 20)	1·13842 (−01)
	e_2		e_2
8×16	−2·12949 (−05)	—	—
16×32	−2·14441 (−05)	(24, 16)	−2·1365 (−05)
32×64	−2·14674 (−05)	(30, 20)	−2·14162 (−05)
	e_3		e_3
8×16	1·4331 (−08)	—	—
16×32	1·8766 (−08)	(24, 16)	2·29225 (−08)
32×64	2·0998 (−08)	(30, 20)	2·30308 (−08)
	c_2		c_2
—	—	(12, 12)	9·18305 (−04)
8×16	1·0024 (−03)	(16, 16)	9·18349 (−04)
16×32	9·4220 (−04)	(24, 16)	9·18355 (−04)
32×64	9·2468 (−04)	(30, 20)	9·18364 (−04)
	c_3		c_3
—	—	(12, 12)	−8·3089 (−07)
8×16	−4·4897 (−07)	(16, 16)	−8·3036 (−07)
16×32	−6·30584 (−07)	(24, 16)	−8·3007 (−07)
32×64	−7·31308 (−07)	(30, 20)	−8·3002 (−07)

TABLE 8. Comparison of finite-difference with direct (Galerkin) evaluation. $A = 2$.

consideration, so we did not explore this possibility. We did, however, make a brief comparison with finite-difference techniques which exploit the availability of direct Poisson solvers to invert the resulting matrices directly. These were, in general, disappointing. Table 8 gives results of a few trials on the first few c_n and e_n from (4.4) and (4.5). Even with Richardson extrapolation, the direct methods and fourth-order-accurate finite differences did not yield comparable accuracy for a comparable computation time. (A direct 32×64 Poisson solve took about as much time as direct evaluation using $(M, N) = (30, 20)$ spectral resolution.) The comparison in table 8 also gives a measure of the accuracy obtained by the direct evaluation.

REFERENCES

BAKER, G. A. 1965 *Adv. Theor. Phys.* **1**, 1.

BANKVALL, C. 1974 *Wärme- und Stoffübertragung* **7**, 22.

CALTAGIRONE, J. P. 1975 *J. Fluid Mech.* **72**, 269.

CHAN, B., IVEY, C. & BARRY J. 1970 *J. Heat Transfer* **2**, 21.

CLOUPEAU, M. & KLARSFELD, S. 1973 *Appl. Optics* **12**, 198.

COMBARNOUS, M. & BORIES, S. 1975 *Adv. Hydrosci.* **10**, 231.

CORMACK, D., LEAL, L. G. & IMBERGER, J. 1974 *J. Fluid Mech.* **65**, 209.

DOMB, C. & SYKES, M. F. 1957 *Proc. Roy. Soc.* A **240**, 214.

FROST, P. A. & HARPER, E. 1976 *SIAM Rev.* **18**, 62.

GAUNT D. S. & GUTTMAN, A. J. 1974 In *Phase Transitions and Critical Phenomena* (ed. C. Domb & M. S. Green), vol. 3, p. 181. Academic Press.

GILL, A. E. 1966 *J. Fluid Mech.* **26**, 515.

HOLST, P. & AZIZ, K. 1972 *Can. J. Chem. Engrs* **50**, 232.

HORNE, R. 1975 Transient effects in geothermal convective systems. Ph.D. thesis, University of Auckland.

HORNE, R. & O'SULLIVAN, M. 1974 *J. Fluid Mech.* **66**, 339.

KASSOY, D. & ZEBIB, A. 1975 *Phys. Fluids* **18**, 1649.

KLARSFELD, S. 1970 *Rev. Gén. Thermique* **9**, 1403.

PALM, E., WEBER, J. & KVERNVOLD, O. 1972 *J. Fluid Mech.* **54**, 153.

QUON, C. 1977 *J. Heat Transfer* **99**, 340.

STEWARTSON, K. 1976 *Quart. J. Mech. Appl. Math.* **29**, 377.

STRAUS, J. 1974 *J. Fluid Mech.* **64**, 51.

VAN DYKE, M. 1974 *Quart. J. Mech. Appl. Math.* **27**, 423.

VAN DYKE, M. 1977 In *Singular Perturbation Boundary Layer Theory* (ed. A. Dold & B. Eckmann). Springer.

VAN DYKE, M. 1978 *J. Fluid Mech.* **86**, 129.

WEBER, J. 1975 *J. Heat Mass Transfer* **18**, 569.